Geomechanics and Engineering, *Vol. 38, No. 1 (2024) 15-28*
https://doi.org/10.12989/gae.2024.38.1.015

Deformation mechanisms of shallow-buried pipelines during road widening: Field and numerical investigation

Long Chen[1a], Chenlei Xie[1b], Zi Ye*[1,2], Yonghui Chen[1], Zhewei Chai[1] and Yun Li[1]

[1]*Key Laboratory of Ministry of Education for Geomechanics and Embankment-Engineering, Hohai University, Nanjing, China*
[2]*Suzhou Research Institute, Hohai University, Suzhou 215000, China*

(*Received December 14, 2023, Revised May 22, 2024, Accepted June 19, 2024*)

Abstract. The rapid development of the economy has compelled the widen of highways, and the main challenge of this undertaking lies in the uneven settlement of road embankments. Through field and numerical experiments, this study explores the deformation mechanism of shallow buried pipelines due to road widening. The utilization of Plaxis3D software, which is adapt at simulating complex engineering geological conditions, enables the simulation of the settlement of both the central and right-side road embankments. Comparing with other numerical software such as ABAQUS and COMSOL, Plaxis provided more constitutive models including HS, HSS and Hoek-Brown model. The work concludes that the uneven settlement of road cross-sections is positively correlated with the horizontal distance from the pipeline, with a maximum settlement of 73 mm observed after construction. Furthermore, based on the Winkler's assumption, theoretical settlement and stress calculation methods are established. Results indicate that the maximum difference between the calculated values of this formula and simulated values is 1.9% and 7%, respectively. Additionally, the study investigates the stress and settlement of the pipeline's top under different angles to understand its behavior under various conditions. It finds that with traffic loads applied to the new embankment, a lever effect occurs on the lower pipeline, with the fulcrum located within the central isolation zone, leading to a transition in curve type from "single peak and single valley" to "double peak and single valley." Moreover, the settlement of pipelines on both sides of the central isolation zone and the normal stress of the pipeline's top section are symmetrical.

Keywords: FEM analysis; field test; pipeline; road widening

1. Introduction

The two-lane highways in both directions are no longer able to meet the growing traffic demands (Alshboul *et al.* 2021, Shehadeh *et al.* 2024). Therefore, the emergence of widening techniques has changed this situation (Bin *et al.* 2022, Alshboul *et al.* 2024, Shehadeh *et al.* 2024, Chen *et al.* 2020). In fact, adding a new embankment on the basis of the existing embankment will encounter additional stress and deformation under the embankment section (Chen *et al.* 2020), resulting in uneven settlement (Chen *et al.* 2022), longitudinal cracks and pavement damage (David *et al.* 2022) in the widened part and finally affecting the long-term performance of the road. Research indicates that differential settlement is primarily due to differences in the compression deformation characteristics of soft soil at varying consolidation times between old and new roads, (Du *et al.* 2016). which can directly result in more pronounced settlement on the side closer to the embankment. Therefore, it is evident that controlling the settlement difference between old and new embankments is crucial for highway widening and joining projects (Han *et al.* 2007, Al-Shboul *et al.* 2023, Almadi *et al.* 2023).

In fact, the uneven settlement subjected to the road widening engineering not only affects the driving safety and the service life of the road, but also threatens the performance of burying pipelines. The additional soil stress resulted from the new road may lead to the excessive stress (Almasabha *et al.* 2023, Kouretzis and Wu 2021) or the distortion of underground pipelines (Liu *et al.* 2023), resulting in rupture and leakage of pipelines and affecting the normal use of public facilities such as drainage, natural gas, and communications (Liu *et al.* 2023). The underground engineering characteristic of pipelines determines its daily maintenance and reconstruction costs are extremely high, and the investigation on the deformation mechanisms of the pipeline is of great significance. In general, the buried depth of pipeline (Luo *et al.* 2015, Alshboul *et al.* 2023, Almasabha *et al.* 2023, Halalsheh *et al.* 2022, Lv *et al.* 2021), soil physical parameters (Marcotte *et al.* 2019, Alshboul *et al.* 2022, Shehadeh *et al.* 2021, Alshboul *et al.* 2024, Marek *et al.* 2021), especially shear modulus (Marek *et al.* 2021, Alshboul *et al.* 2022, Meng *et al.* 2022, Alshboul *et al.* 2022, Alshboul *et al.* 2021, Mohammadreza *et al.* 2023) are also one of the main factors. In road widening projects, sufficient geological survey and engineering design are required to ensure uniform settlement between the new road and the old road. Reasonable design and construction

*Corresponding author, Post Doctor
E-mail: ziye_1995@163.com
[a]Professor
E-mail: longchenhhu@163.com
[b]Student
E-mail: lyxcl2009@126.com

Copyright © 2024 Techno-Press, Ltd.

ISSN: 2005-307X (Print), 2092-6219 (Online)

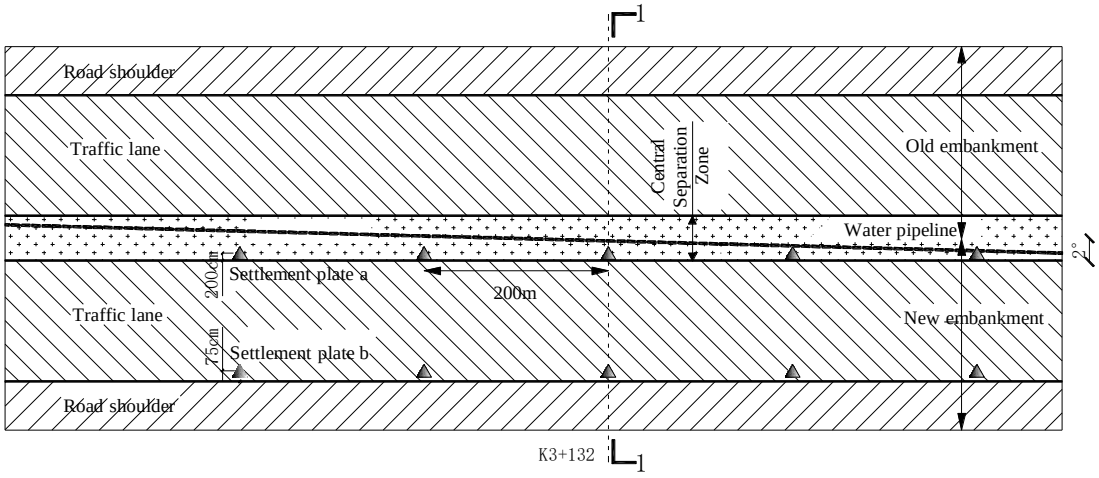

(a) Top view of test section

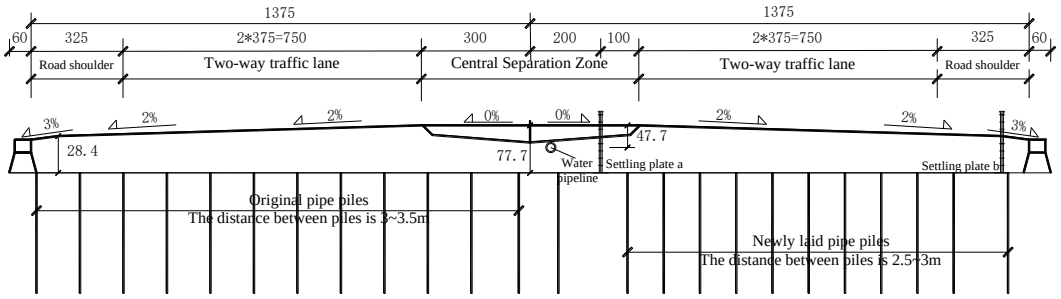

(b) Section 1-1（unit: cm）

Fig. 1 Detail drawing of K3+132.8 section

methods can reduce the additional stress and deformation of underground pipelines (Meng *et al.* 2022, Qin *et al.* 2021, Alshboul *et al.* 2022, Alshboul *et al.* 2021, Wu *et al.* 2019).

In summary, road widening is a continuous endeavor, and it inevitably affects buried pipelines. Besides, existing research articles predominantly concentrate on scenarios where roadbed consolidation is finalized, and the discussion revolves around the assumption of either a 0° (Orynyak *et al.* 2019) or 90° (Yang *et al.* 2022) angle between the pipeline and the road. There is relatively less discussion about scenarios where roadbed consolidation is not yet complete and the angle between the pipeline and the road can be any other value. Therefore, this paper establishes a finite element software model that can match field-measured data. By combining finite element analysis methods with theoretical derivation methods, the paper conducts a detailed analysis of the settlement characteristics at different stages and the settlement and top stress of pipelines with different pipe inclinations. The conclusions drawn from these analyses may enhance the design of buried pipelines and road widening projects, thus improving the safety and cost-effectiveness of infrastructure maintenance.

2. Background

2.1 Site overview

The cross section of K2 + 910 ~ K10 + 790 has the intersection of water pipeline and embankment, and the section at K3 + 132.8 is selected as the typical treatment section. Fig. 1 shows the plan and elevation of the construction site, there is a pipeline buried 0.477 m in depth with an inclination of 2° with the road. This water pipe is made of alloy material with an outer diameter of 0.1 meters.

The new embankment is symmetrically arranged with the old embankment, so their cross-sectional form is the same. The width of the new embankment is 15.35 m and the maximum fill height is 0.77 m. The width of the central divider is 5 m and the width of each side of the curb zone is 0.5 m. The slope of the lane (which single lane width is 3.75 m) and hard shoulder is 3% outward, while the slope of the soil shoulder with a width of 0.75 m is 2% outward.

In order to reduce the soil movement caused by road widening, reinforced prestressed pipe piles with a diameter of 400 mm and a pipe wall thickness of 60 mm were set with a spacing of 2.5 to 3.0 m.

2.2 Geology

Table 1 provides comprehensive physical and mechanical parameters of the soil layer. The surface comprises a 50 cm thick layer of concrete, followed by slag and miscellaneous fill with a cohesion of 5 kPa. The surface layer primarily consists of cement gravel, concrete, and backfill, with a thickness ranging from 0.2 to 0.8 meters.

Table 1 Table of soil parameters

Soil layer	Saturated density γ_{sat}/kN/m^3	Void ratio e	Compression modulus E/MPa	Possion's ratio υ	Cohesion c/kN	Friction angle φ/°	bottom level h/m	k_x m/day	k_Z m/day
①-Surface	24	0.5	200	0.17	2	35	4.5	/	/
②-Slag	19	0.6	9	0.4	3	19	4.3	/	1.73E-01
③-Miscellaneous fill	19	0.8	2	0.2	5	15	3.3	7.69E-05	7.26E-05
④-Clay	17.7	1.11	3	0.35	24	15	1.5	1.24E-04	9.68E-05
⑤-Silt-1	17	1.3	2.3	0.4	12	19	0.1	1.05E-4	7.57E-5
⑥-Silt and sand interlayer	17.7	1.11	2.3	0.4	12	19	-3.7	/	8.99E-2
⑦-Silt -2	17	1.34	2.5	0.35	12	12	-15.1	1.07E-4	7.65E-5
⑧-Powdery clay	18.9	0.824	8	0.42	23	19	-16.6	/	2.25E-1
⑨-Gravel	26.5	0.5	20	0.38	0	40	-29.09	/	/

The lower soil layers consist of silt and clay. The cohesion of the middle soil layer is 12 kPa. Beneath these layers lies a gravel bottom layer, upon which the reinforced prestressed pipe pile depicted in Fig. 1(b) is positioned. The gravel cushion boasts a significantly high elastic modulus of 20 MPa, with a cohesion of 0 kPa, and spans approximately 12.5 meters in thickness.

2.3 Construction sequence

Following the soft soil treatment design on the construction site, the initial step involves setting out and employing the static pressure method to reinforce the foundation using prestressed pipe piles. These piles have a diameter of 400 mm and a pipe wall thickness of 60 mm. Subsequently, upon completion of the pipe pile construction, the surface soil is removed, and steps are excavated along the slope of the old road. These steps have a height of 50 cm and a width of 100 cm. For section K3+132, as shown in Fig. 2 the buried depth of the pipeline is relatively shallow and may even be exposed to the air. Therefore, the excavation elevation should be strictly controlled and temporary support should be set up within a certain range around the pipeline for subsequent demolition work.

2.4 Instrumentation

In order to monitor the safety and stability during the construction process and predict the settlement after construction, settlement plates with dimensions of 50 cm×50 cm×10 mm were installed at the center and right shoulder of the road, as shown in Fig. 1. In this section, two burial points are arranged every 200 m for monitoring purposes. Settlement monitoring is required at least once daily during the loading process. Following three days of unloading, monitoring frequency shifts to every 3-15 days, determined by the settlement rate. Observations must adhere to fourth-level measurement accuracy standards, ensuring that the height difference between adjacent observation points does not exceed 1 mm.

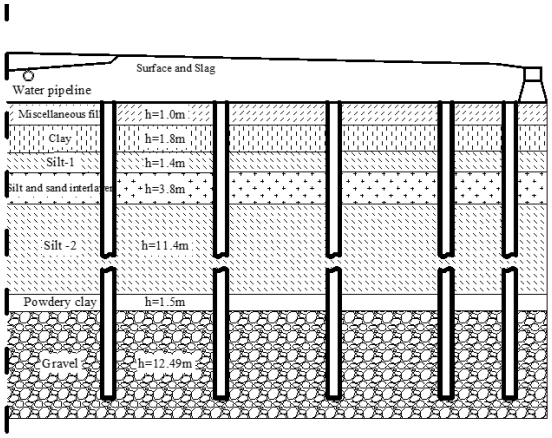

(a) Geological section

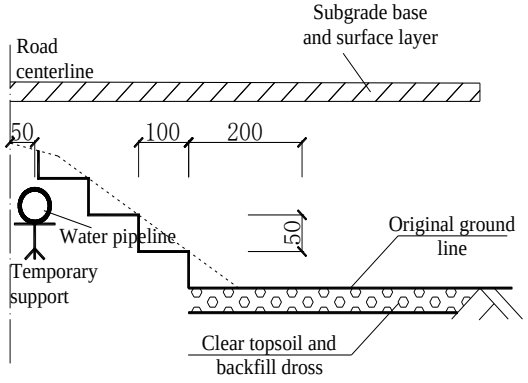

(b) Local drawing of pipeline map

Fig. 2 Schematic diagram of grading and pavement practices (unit: cm)

3. Numerical modeling

3.1 Numerical mesh and boundary condition

Plaxis3D software is used to investigate the deformation mechanisms of shallow-buried pipelines during road widening. The roughness factors of the pile and soil are set to 0.5 and 1.0, respectively, with unit distribution set to "medium". Check for

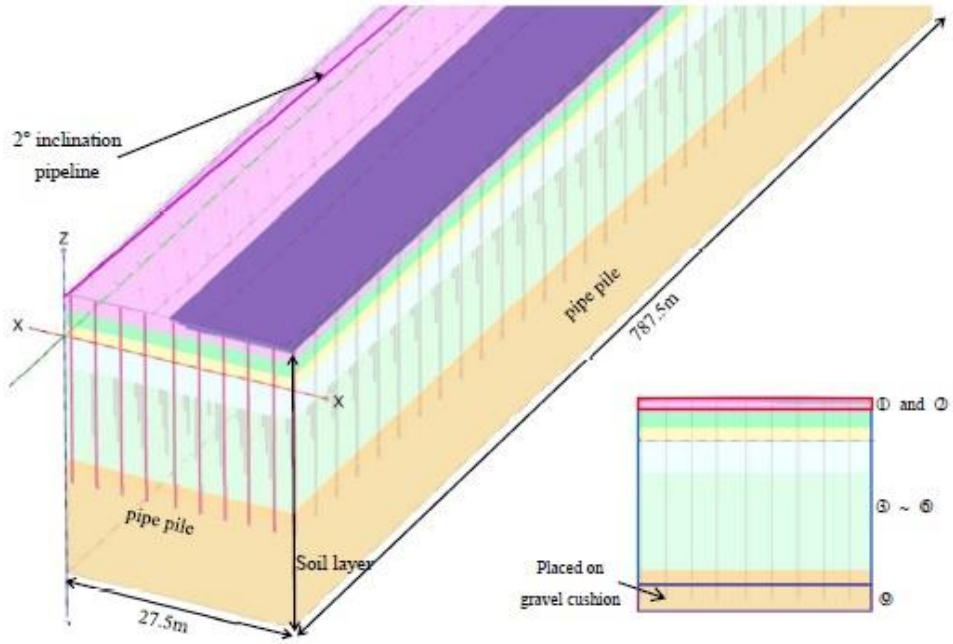

Fig. 3 Plaxis3D model diagram

Table 2 The value method of soil HSS model parameters recommended by Shanghai

Soil layer	E_{oed}^{ref}/MPa	E_{50}^{ref}/MPa	E_{ur}^{ref}/MPa	G_0^{ref}/MPa	$\gamma_{0.7}/10^{-4}$
Clay	$0.9E_{s1-2}$		$6E_{oed}^{ref}$	(2.5~4.9) * E_{ur}^{ref}	1.5~9.0
Powdery clay					

"enhanced mesh refinement", global scale factor set to "1.2", and minimum unit size factor set to "5e-3". The numerical model is shown in Fig. 3.

The length of the model is equal to the width of the road, which is 27.5 m. The height of the model is equal to the height from the top of the fill to the bottom of the gravel layer, which is 34.167 meters. The model deformation conditions in the other five directions are set to "fixed", except that Z_{max} (top boundary of model) is set to "free".

3.2 Soil model and model parameters

Common soil models used in FEM analysis include Mohr-Coulomb model, hardening soil model (HS), hardening soil model with small strain stiffness (HSS) and Cambridge model. The existing researches shows that the deformation prediction value obtained by MCC model (Yasuhiko *et al*. 2023) and HS model (Marek *et al*. 2021, Ye *et al*. 2023) is higher than that of HSS model. The numerical results obtained by HSS model are in better agreement with the measured data than M-C model (Zhao *et al.* 2019). In fact, the HSS model was first proposed by Benz (Zhang *et al*. 2023). In fact, soils in most of the actual engineering are in the small strain deformation range under strict deformation control (Zhang *et al.* 2022), the HSS model can consider the nonlinear elastic characteristics and stress-related characteristics of the soil in the small strain stage. Therefore, compared with other models, the deformation value calculated by HSS model is closer to the measured value, which is more suitable for engineering problems with strict deformation requirements. Hence, HSS model is utilized in the following research.

However, the HSS model parameters are numerous. From the perspective of theoretical formulas, (Hardin and Black 1969) provided a method for determining the value of G_0^{ref}; Xie *et al*. (2017) provided a method for determining the value of $\gamma_{0.7}$. From the perspective of engineering experience values, there are often differences in the multiple relationship between HSS model parameters in different regions. Dong *et al.* (2023) provided the parameter differences between Changzhou and Nanjing. In summary, the selection of HSS models should not only consider the project location, but also combine engineering experience and relevant specifications. This paper presents the method for determining parameter values, as depicted in Table 2.

The soil parameters involved in the table are necessary to explain: E_{oed}^{ref} is the tangent modulus of consolidation test, and the elastic modulus is generally taken. E_{50}^{ref} is the secant modulus of triaxial consolidated drained shear test, and generally takes the compression modulus; E_{ur}^{ref} is the unloading and reloading modulus of the triaxial consolidated drained unloading and reloading test, which is generally three times the elastic modulus. In the above table, take E_{oed}^{ref} and E_{50}^{ref} equal to 0.9 times the compression modulus; E_{ur}^{ref} is equal to 6 times the compression modulus. G_0^{ref} is the reference initial shear modulus of the small strain

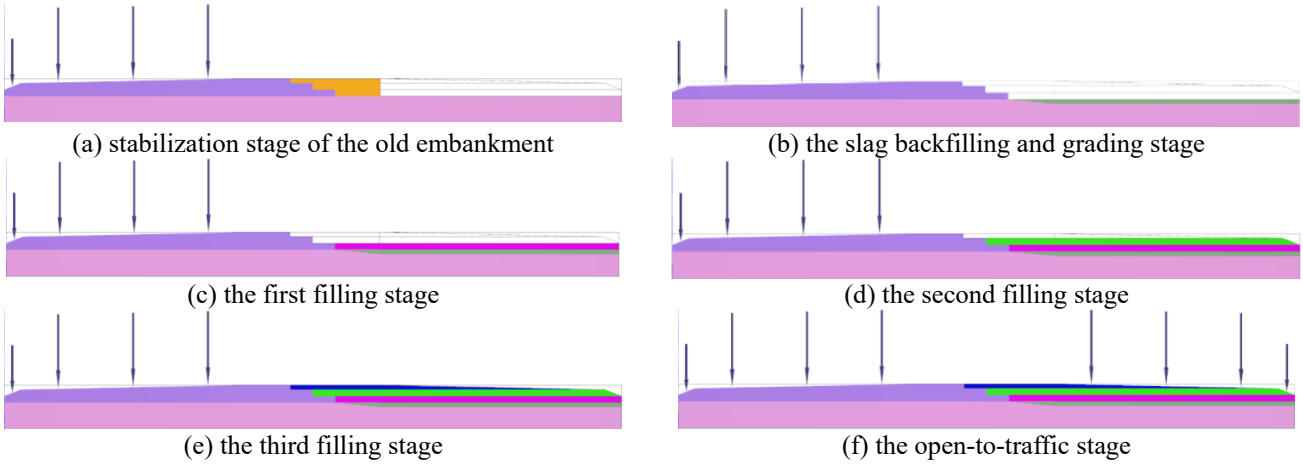

(a) stabilization stage of the old embankment (b) the slag backfilling and grading stage

(c) the first filling stage (d) the second filling stage

(e) the third filling stage (f) the open-to-traffic stage

Fig. 4 Model diagrams for different stages

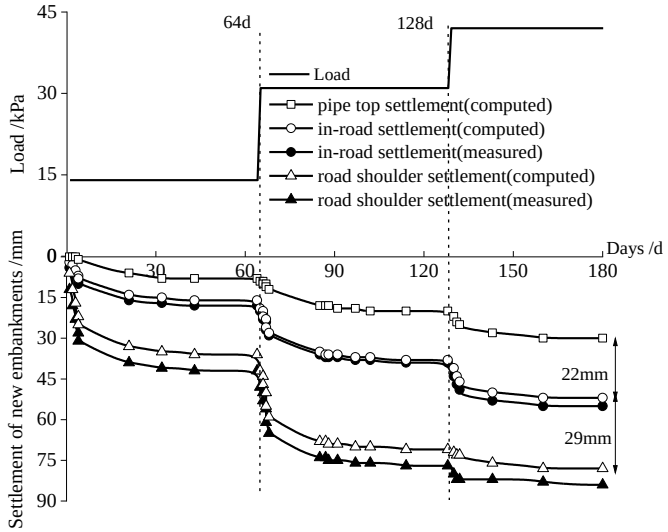

Fig. 5 Load settlement relation curve of embankment in graded filling stage

stiffness test, which is the shear modulus of the smaller strain, and generally takes 3 times of the unloading elastic modulus; $\gamma_{0.7}$ is the corresponding shear strain when the secant shear modulus decays to 0.7 times. In the above table, G_0^{ref} takes 2.5 ~ 4.9 times E_{ur}^{ref}; take $\gamma_{0.7}$ about (1.5 ~ 9.0) $\times 10^{-4}$.

3.3 Numerical modelling procedures

In the modeling stage, the HSS model is used to simulate the soil, and the "beam element" is used to simulate the pipeline. They are modeled through the "boreholes" option in the "Soil" menu and the "pre-buried beams" option in the "Structure" menu, respectively. The width of the model is equal to the width of the road, i.e., 27.5 m. The length of the model is equal to the projection length of the pipeline in the road direction, i.e., 787.5 m.

In order to recreate the real construction process, 10 stages are set in the "phased construction" menu (the model diagram for the key stages is shown in Fig. 4). Including the stabilization stage of the old embankment, the slag backfilling and grading stage, a total of three filling stages and corresponding soil consolidation stages after each filling stage, the open-to-traffic stage and the post-construction settlement observation stage

It's worth noting that the filling height remains relatively consistent across all three filling stages. and it can be seen from the figure that the traffic load on the carriageway is different from that on the earth and hard shoulder. This divergence arises from the prescribed specifications: the traffic load on the carriageway is set to 15.06 kN/m^2, and the traffic load on the earth shoulder and hard shoulder is set to 9.6 kN/m^2.

4. Simulation results

4.1 Verification of the model and analysis

As shown in Fig. 1(a), settlement plates on sites were placed in the middle of the road and at the shoulder of the road. The settlement of the two settlement plates measured in the field will be compared with that of the top of the pipeline in the numerical model, as shown in Fig. 5. It is important to note

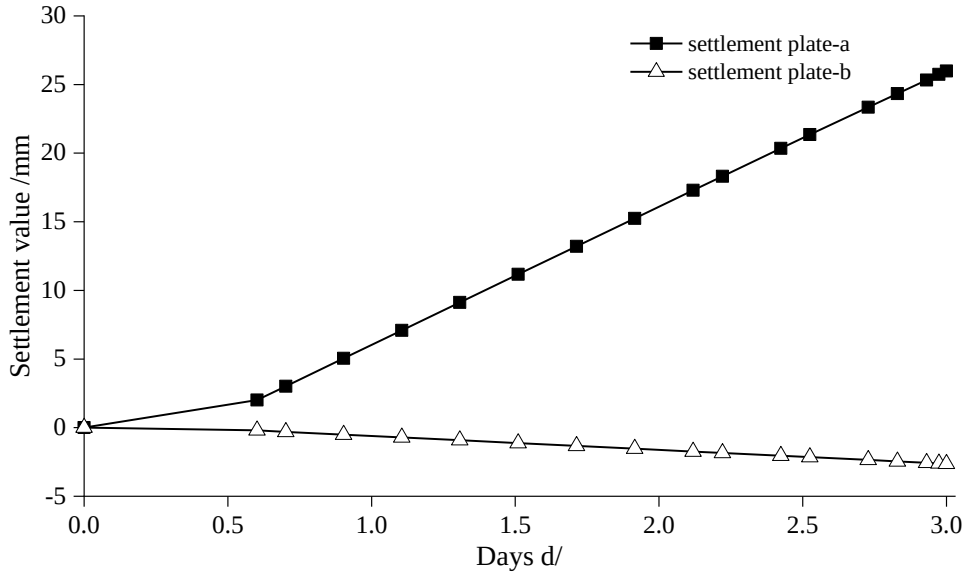

Fig. 6 Comparison diagram of road pipeline settlement in grading stage

that the site construction is divided into three loading stages, each approximately 0.25 meters in height. The loading period spans 4 days, followed by a consolidation time of 60 days.

With the graded application of load, the settlement of road and shoulder also shows a corresponding upward trend. Comparing the simulated results and experimented results at the same position, it can be found that the settlement error in the road is about 2 mm, and the settlement error of the shoulder is about 5 mm. Hence, the established FEM model and parameter selection are reasonable. Furthermore, it can be found that the settlement value of the pipeline is the smallest, approximately 30 mm, followed by the road with a settlement value of around 52 mm, and finally, the shoulder exhibits the largest settlement value at about 81 mm. This discrepancy can be attributed to the pipeline's inherently greater elastic modulus compared to the soil, resulting in lesser deformation under the same load. Additionally, the older embankment has undergone a complete drainage process, causing the soil in the center of the road to settle lower than the shoulder soil under identical loading conditions.

4.2 Analysis of settlement characteristics in different stages

4.2.1 The slope stage

As mentioned earlier, maintaining access to the existing road section is imperative throughout the embankment widening procedure. As shown in Fig. 6, with the central separation as the symmetry axis, the old and new embankments, initially in equilibrium, underwent unloading as the topsoil was excavated from the slope. This process resulted in an upward bulge at the junction of the old and new embankments due to the traffic load on the old road however, the rightmost side of the new embankment still maintained a downward settlement trend.

The height of the slope step and the width of the tread can be referred to Fig. 2 Assuming a slope period of 3 days, we compare the settlement at "point a" located at 2 m from the separation midpoint, and "point b" situated 0.75 m from the right shoulder. From Fig. 6, It's apparent that the settlement-time relationship during the slope process follows an approximately linear pattern. After the slope ends, “point a” undergoes an upward rise of around 26mm, whereas "point b" settles downward by approximately 3mm. This discrepancy is due to the proximity of "point a" to the consolidated and stabilized side of the old embankment, resulting in better soil characteristics and a rebound effect caused by the unloading action (slope). On the other hand, "point b" is situated on the shoulder of the new embankment, where lower soil remains in a looser state. Consequently, the traffic load of the old embankment causes the soil at "point b" settle larger.

4.2.2 Loading and traffic stages

In order to explore the settlement variation law of subgrade at the height of pipeline center line (Z = 4.78 m) at different stages, the three stages of the first loading stage, the third loading stage and the post-construction settlement of 15 years are shown in Fig. 7. To investigate the settlement variation pattern of the subgrade at the height of the pipeline center line (Z = 4.78 m) across various stages, Fig. 6 illustrates three stages: the initial loading stage, the third loading stage, and the settlement observed after 15 years of construction. In the model, 17 calculation points were selected, which were − 2.7 m, − 1.7 m, − 0.7 m, − 0.1 m (the coordinates of the leftmost point of the pipeline), 0 m, 0.1 m (the coordinates of the rightmost point of the pipeline), 0.3 m, 1.3 m, 2.3 m, 3.3 m, 4.3 m, 5.3 m, 6.3 m, 7.3 m, 8.3 m, 9.3 m and 10.3 m respectively.

The settling of the old embankment during construction was minimal, measuring less than 10 mm, owing to prior consolidation. The application of a 14 kPa-load resulted in the settling of the pipe adjacent to the new embankment. Raising the load to 42 kPa led to minimal settlement of the pipe beneath the central separation, while significant settling occurred beneath the new embankment,

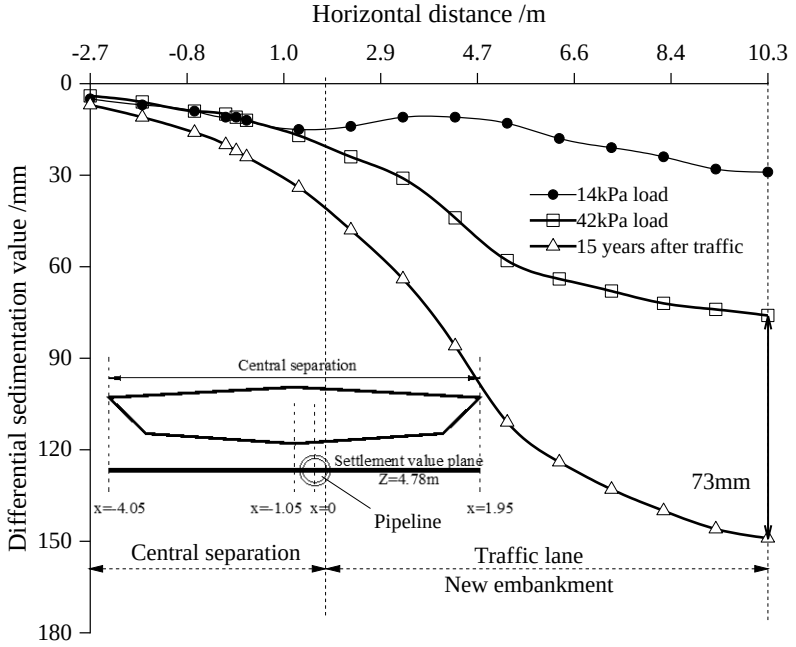

Fig. 7 Uneven settlement curve of road cross section during embankment construction

reaching a maximum differential settlement of 47 mm.After completion of graded filling and 15 years of traffic on the new road, compared to the ″42 kPa load″ curve, the pipe beneath the central separation experienced a settlement of approximately 2 mm. However, significant settlement occurred beneath the new embankment, with greater relative settlement as the distance from x=0 m increased, reaching a maximum difference of 73 mm.

This indicates that after widening the embankment, the settlement at the center point of the road is relatively small, and the settlement at the shoulder is relatively large, resulting in an increase in the transverse slope of the road after widening (consistent with the conclusion of Jia *et al.* (2024)).

5. Theoretical calculation model of stresses in pipe sections

In the preceding section, settlement variations across various loading consolidation stages were analyzed using the finite element method. This section will now establish a calculation model to assess the settlement and stress changes of the pipeline cross-section.

5.1 Basic assumptions

The following assumptions are provided to simplify the mathematical model:

(1) The old embankment soil shoulder portion as a fixed end restraint.

(2) The central separation section is completely unstressed.

(3) In this section, the Winkler (Zheng *et al*. 2021) foundation model is chosen, and the bed reaction coefficient "k" and the concentration coefficient are considered, where "k" takes the value of 3×10^4 and the concentration coefficient takes 1.23.

5.2 Load calculation

The force on the pipe is actually composed of two parts: the force "q" at the top of the pipe vertically downward and the force "Q" perpendicular to the pipe upward. Where "q" is mainly composed of the traffic load generated by the new and old embankment and the self-weight load of the soil above the pipe, which is calculated as "q=26.2 kN/m^2". Since the central isolation zone part is not stressed in the actual problem, the pipe settlement generated by "q" is simplified to "$y_{tl}(x)$" and "$y_{cl}(x)$" in Fig. 8, where the subscript "tl" is the abbreviation of traffic load; "cl" is the abbreviation of central isolation zone load. "Q" can be considered as the bed reaction force, and according to Winkler's assumption, the magnitude of "Q" is related to the settlement of the foundation at that point ($\sum_{i=1}^{3} y_i$) is proportional, so "Q" is assumed to be a parabolic load.

The following formula parameters are necessary to explain: "a" indicates the width of the load action; "x" indicates different locations in the range of [0, a]; "q" indicates the uniform load on the top of the pipe under the action of the ground vehicle and when the concentration factor is considered; "EI" indicates the bending stiffness of the pipe; "L" indicates the actual length of the pipe; "Q" indicates the bed reaction force and "k" indicates the bed reaction force coefficient, however, this formula takes a simplified treatment: the variation of "k" values in different soil layers is not considered; "W_z" indicates the flexural section coefficient

$$y_{tl}(\mathrm{x}) = \frac{-qx^2(\mathrm{x}^2 - 4\mathrm{Lx} + 6\mathrm{L}^2)}{24EI} \tag{1}$$

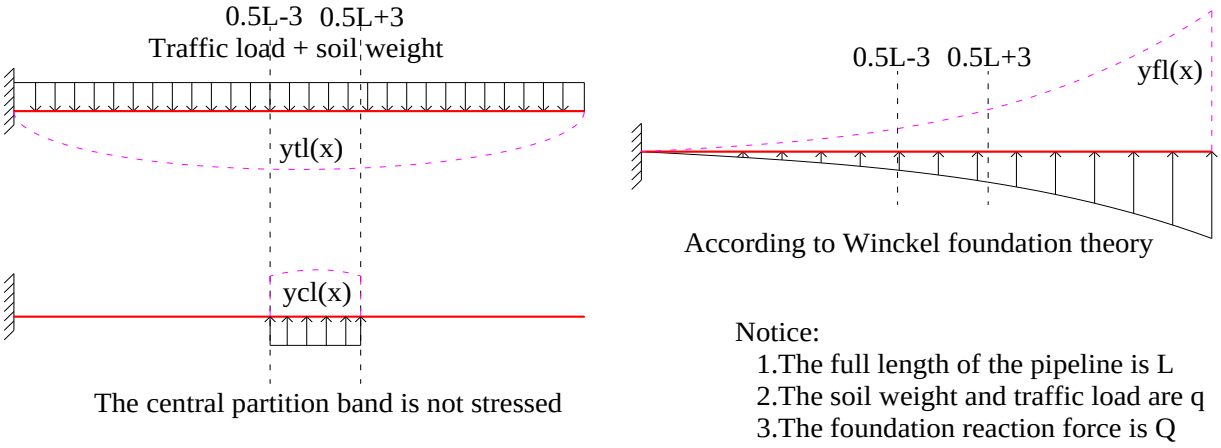

Fig. 8 Pipeline stress diagram

$$y_{cl}(\mathrm{x})=\begin{pmatrix}\dfrac{qx^2}{EI}(1.5\mathrm{L}-\mathrm{x}),0\le \mathrm{x}\le 0.5\mathrm{L}+3\\ \dfrac{qL^2}{4EI}(3\mathrm{x}-0.5\mathrm{L}),0.5L+3\le \mathrm{x}\le \mathrm{L}\end{pmatrix} \tag{2}$$

$$y_{fl}(\mathrm{x})=\int_0^L\frac{Qx^2}{6EI}(3\mathrm{a}-\mathrm{x})\,\mathrm{da}=\frac{Qx^2L}{12EI}(3\mathrm{L}-2\,\mathrm{x}) \tag{3}$$

The derivation of Eq. (1) can refer to the form of the deflection curve of a cantilever beam subjected to uniform load in the appendix of Mechanics of Materials. The derivation of Eq. (2), considering the possible forms of its deflection curve, is based on the integration equation of the segmental deflection curve when subjected to the concentrated load (Zhou *et al.* 2018). Eq. (3) assumes that $y_{fl}(x)$ is generated by "Q" alone and "Q" is independent of all variables except "x". So integration of the length of action a of the uniform load "Q" gives $y_{fl}(x)$, where "*fl*" is the abbreviation of foundation reaction load

5.3 Theoretical derivation

The Eq. (4) is based on the formula given by the Winkler foundation model. By combining Eqs. (1)-(4), the $y_{fl}(x)$ generated by the foundation reaction can be obtained, as shown in Eq. (5). The the total settlement value Σy of the pipeline is shown in Eq. (6). By combining Eqs. (5) and (6), the settlement value of the pipeline can be obtained, as shown in Eq. (7)

$$Q=k(y_{tl}+y_{cl}+y_{fl}) \tag{4}$$

$$y_{fl}(\mathrm{x})=\begin{pmatrix}\dfrac{q\left[-x^4+(4\mathrm{L}-24)x^3+(36\mathrm{L}-6\mathrm{L}^2+216)x^2-(216\mathrm{L}+648)x+(645+324\mathrm{L})\right]}{24EI},0\le 0.5L\le 3\\ \dfrac{q(-x^4+4\mathrm{L}x^3-6\mathrm{L}^2x^2+18L^2\,\mathrm{x}-3\mathrm{L}^3-54\mathrm{L}^2)}{24EI},0.5L+3\le x\le L\end{pmatrix} \tag{5}$$

$$\sum y=y_{tl}(\mathrm{x})+y_{fl}(\mathrm{x})+y_{cl}(\mathrm{x}) \tag{6}$$

$$\sum y(\mathrm{x})=\begin{pmatrix}\dfrac{q\left[-x^4+(4\mathrm{L}-24)x^3+(36\mathrm{L}-6\mathrm{L}^2+216)x^2-(216\mathrm{L}+648)x+(645+324\mathrm{L})\right]}{4\left[6EI-kx^2L(1.5\mathrm{L}-\mathrm{x})\right]},0\le 0.5L\le 3\\ \dfrac{q(-x^4+4\mathrm{L}x^3-6\mathrm{L}^2x^2+18L^2\,\mathrm{x}-3\mathrm{L}^3-54\mathrm{L}^2)}{4\left[6EI-kx^2L(1.5\mathrm{L}-\mathrm{x})\right]},0.5L+3\le x\le L\end{pmatrix} \tag{7}$$

Then Eq. (8) is substituted into Eq. (7) to obtain Eq. (9), which is the positive stress curve considering the prior consolidation of the old embankment and the bed reaction force. With this curve equation, the bending positive stress values at the top of the pipe at different locations can be solved when the pipe length and other material parameters are known

$$\sigma=\frac{-4EI}{W_zL^2}\sum y \tag{8}$$

$$\sigma(\mathrm{x})=\begin{pmatrix}\dfrac{q\left[-x^4+(4\mathrm{L}-24)x^3+(36\mathrm{L}-6\mathrm{L}^2+216)x^2-(216\mathrm{L}+648)x+(645+324\mathrm{L})\right]}{\left[6EI-kx^2L(1.5\mathrm{L}-\mathrm{x})\right]W_zL^2},0\le 0.5L\le 3\\ \dfrac{q(-x^4+4\mathrm{L}x^3-6\mathrm{L}^2x^2+18L^2\,\mathrm{x}-3\mathrm{L}^3-54\mathrm{L}^2)}{\left[6EI-kx^2L(1.5\mathrm{L}-\mathrm{x})\right]W_zL^2},0.5L+3\le x\le L\end{pmatrix} \tag{9}$$

5.4 Comparison of results

In this paper, the pipe settlement and the positive stress at the top of the pipe at seven points (0.75 m, 4.75 m, 8.75 m, 12.75 m, 16.75 m, 20.75 m and 26.75 m) were solved by finite element software and compared with the calculated results of Eqs. (7) and (9). The results are shown in Figs. 9 and 10, respectively. As can be seen from Fig. 9, the x-axis of the settlement value of the pipeline presents a fluctuating trend, with the smallest settlement value 129 mm at the horizontal position 12.75 m and the maximum settlement at the middle of the new embankment (about 20.75 m) and the middle of the old embankment (about 4.75 m).

The central isolation zone is not stressed, and the settlement value is small, whereas the new and old embankments have undergone settlement due to traffic loads. At the central separation zone (12.75 m), the theoretical calculation results align with the software-generated results, both measuring 129 mm. At 5.5 m, the theoretical method yields a settlement value of 156 mm, closely matching the software-calculated value of 153 mm. Similarly, at 22.5 m, the theoretical calculation produces a settlement value of 156 mm, consistent with the software-derived value of 153 mm. It's evident that the theoretical method effectively fits the unstressed portion, but its fitting effectiveness is lacking for the lower section of the

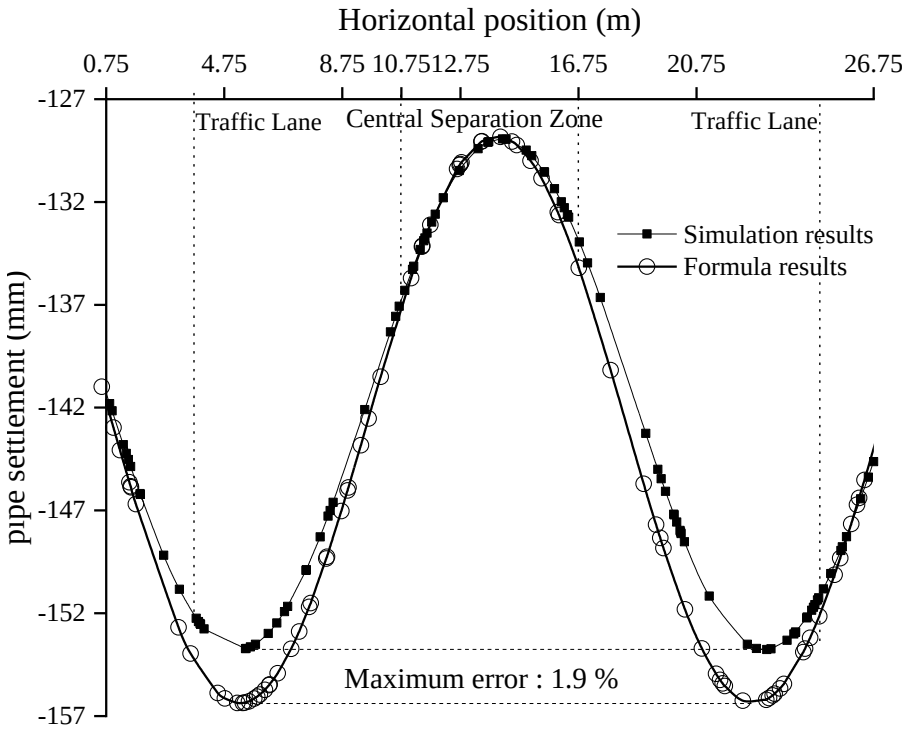

Fig. 9 pipeline settlement comparison curve

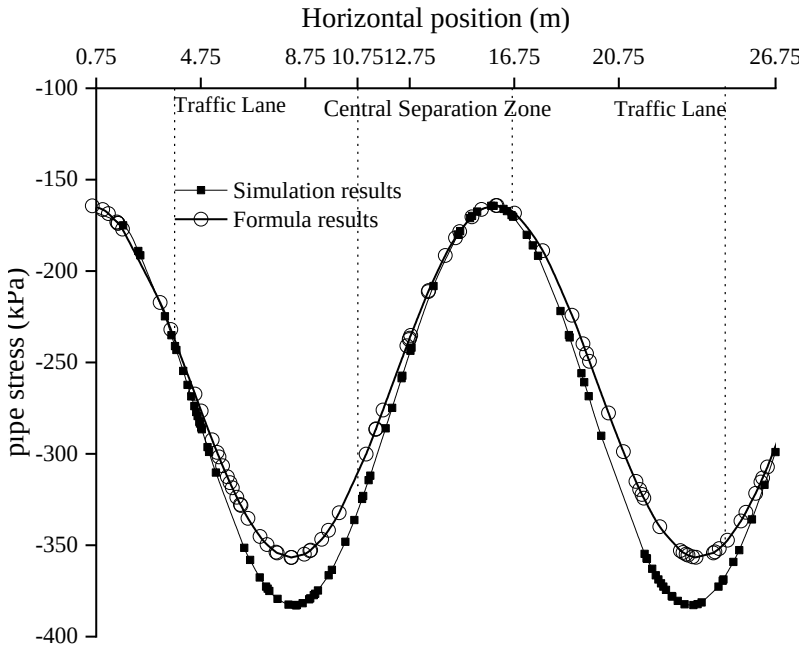

Fig. 1 Normal stress comparison curve of 2 ° pipe section

carriageway. The maximum error of 1.9% falls within the project's acceptable range.

Fig. 10 presents a comparison between the theoretical method results and the software simulation results for pipeline stress at a 2° dip angle. The results demonstrate a close correspondence between the theoretical outcomes and the simulation results, particularly within a range of 4.75 meters from the old embankment and within the central area of the central isolation zone. For the lane range of old embankment and new embankment, the comparison results are relatively poor: for the old embankment, the maximum difference between the results is about 8.3 m, and the results are-356.7 kPa and-382.7 kPa, respectively; for the new embankment, the maximum difference between the results is about 23.75 m, and the results are -356.6 kPa and-382.8 kPa, respectively, with an error of less than 7%. In summary, the error for settlement between simulation method and the theoretical method is 1.9%, and the error for

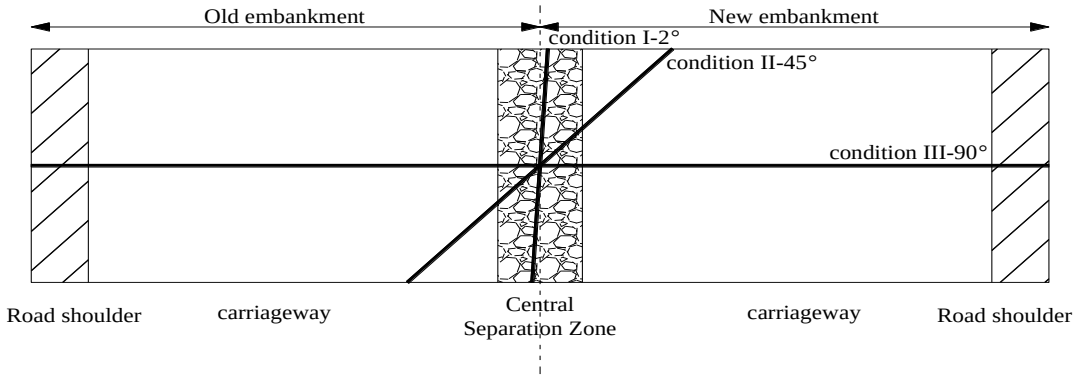

Fig. 11 Pipeline route map

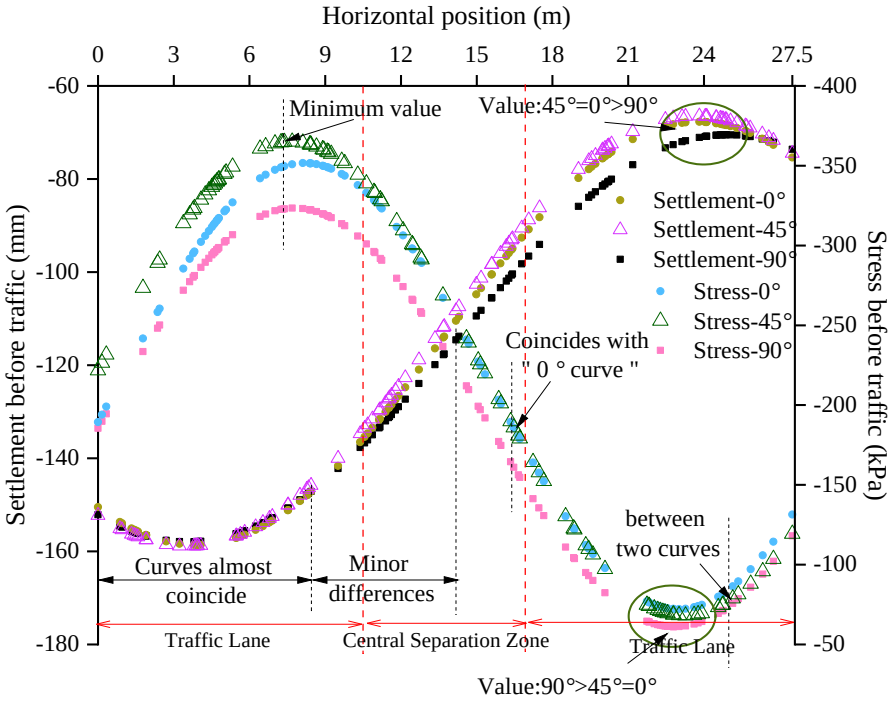

Fig. 12 Comparison curves of settlement stress of pipelines with different inclination angles before traffic

the normal stress of the pipe top section is less than 7%, which can illustrate the applicability of the theoretical method to calculate the settlement stress of buried pipelines.

The comprehensive settlement and stress calculation results indicate a notable alignment between the theoretical and simulation outcomes, barring minor deviations. In practical engineering scenarios, armed with pertinent road parameters, the force and settlement of buried pipelines can be promptly computed. This obviates the need for cumbersome on-site measurements or intricate numerical simulations, streamlining the decision-making process in practical applications.

6. Effects of pipe inclination conditions on settlements and stresses

Most of the discussions in the existing articles are based on the study of the force and deformation characteristics of the pipe at a specific angle However, it's evident that in actual engineering scenarios, the angle between the road and the pipe can vary widely from 0° to 90°, as shown in Fig. 11. Given the issues mentioned above, this section delves deeper into the force and deformation characteristics of the pipe at 0°, 45°, and 90° angles. These characteristics are graphically represented as curves and the results are shown in Figs. 12 and 13.

Fig. 12 shows the variation curves of the top settlement and the normal stress of the pipe top section with different inclination angles after the completion of the construction. It can be found that the settlement and normal stress of the pipeline show the same change rule from the old embankment to the new embankment side. The settlement and stress of the old embankment side are smaller compared with that of the new embankment side.

Further comparison of the influence of pipeline inclination angle on settlement curve reveals that on the side of the old embankment, the settlement is the smallest

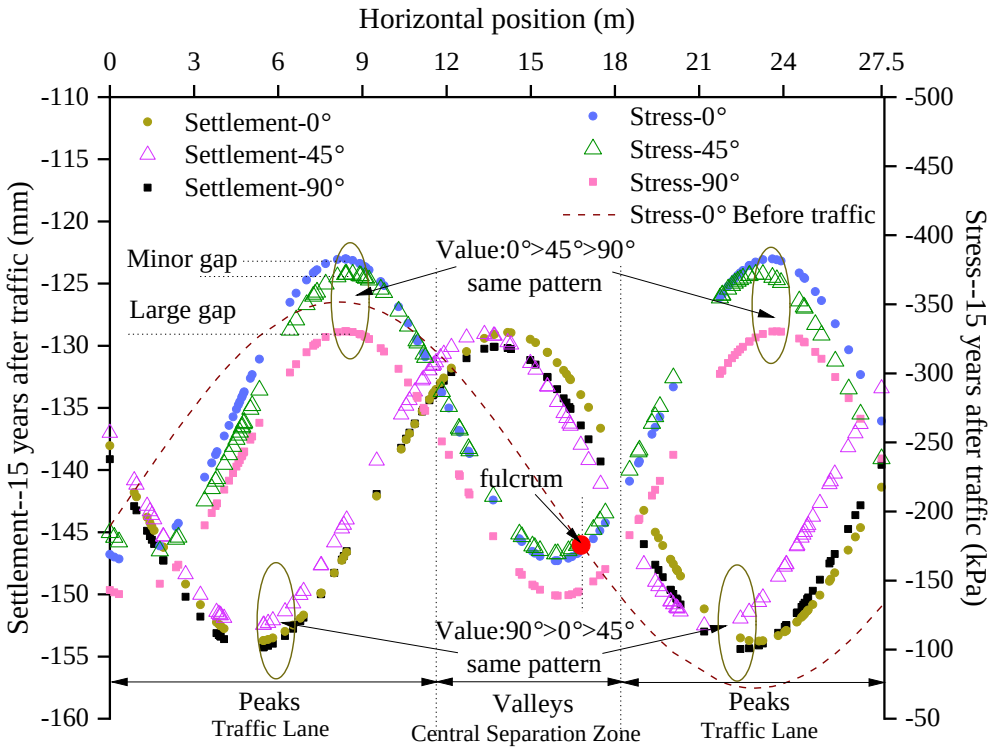

Fig. 13 Comparison curves of settlement stress of pipelines with different inclination angles after 15 years

when the inclination angle is 45°, followed by 0°, and the largest at 90°. In the lower part of the central isolation zone, the settlement curve gradually reduces to zero when the inclination angle is 45°. On the side of the new embankment, the settlement curve for a 45° inclination angle falls between 0° and 90°, with minimal differences among the three curves. It can be found that for the settlement of the pipe top with different inclination angles after the completion of the construction, when the pipeline is perpendicular to the forward direction of the road (90°), the pipeline is most affected by the construction and the settlement is also the largest. Conversely, when the pipeline is parallel to the road (0°), its length within the embankment minimizes the construction impact, resulting in negligible settlement. At an inclination angle of 45°, the settlement change of the pipeline in the perpendicular direction to the road is most significant.

In view of the stress curve, the normal stress on the top section of the pipeline remains largely independent of the pipeline-road angle. Generally, the stress curves align on the old embankment side for different angles, with a slight deviation occurring in the lower part of the central isolation zone. The largest deviation is observed on the new embankment side, although it remains below 20 kPa. Notably, the pipe with a 45° angle experiences the highest normal stress on the new embankment side, followed by the pipe with a 0° angle, while the pipe with a 90° angle experiences the lowest stress. This phenomenon suggests that the criterion of "greater settlement leads to greater stress" is not fulfilled on the new embankment side. The reason is that the side of the new embankment is affected by the graded filling in the construction, so it has a large settlement, but the pipe top stress is mainly affected by the earth pressure and the upper load. The filling height in the actual project is small and there is no traffic load, the pipe top stress is small.

Fig. 13 illustrates the settlement and stress variation curves of the pipe's top section with different inclination angles after 15 years of opening to traffic. The curves exhibit a wave-like pattern beneath the embankment, with peaks located at the central isolation belt and troughs at the lower part of the carriageway.

Comparison of the impact of pipeline inclination angles on settlement and stress reveals that, the settlement is smallest at a 45° angle, followed by 0°, and largest at 90° on the old embankment side. This pattern remains consistent with the pre-traffic curves. Similarly, the settlement curve follows the same trend at the new embankment, with the smallest settlement occurring at the 45° angle, followed by 0°, and the highest at 90°. Notably, the settlement difference between different angles is quite obvious. In conclusion, when the embankment is widened and completely consolidated over time, the settlement of the pipeline beneath the central isolation zone remains nearly constant regardless of the inclination angle. However, for the pipeline situated at the lower part of the carriageway, the settlement pattern shows a consistent trend of minimum settlement at 45°, followed by 0°, and maximum settlement at 90°. Additionally, even after 15 years, the settlement difference on the new embankment is still greater than that on the old embankment.

For the stress curve, the new and old embankments are completely symmetrically distributed, that is, 0° is the largest, 45° is the second, and 90° is the smallest. Among

them, the stress difference between 0° and 45° is very small, about 15 kPa, and the stress difference between 45° and 90° is large, about 40 kPa. In the lower part of the central isolation zone, the 45° pipe stress will be slightly larger than the 0° pipe stress, but the difference is negligible. That is to say, for the consolidated and stabilized embankment the normal stress of the section at the top of the buried pipeline is almost positively correlated with the angle, in which the larger the angle, the greater the normal stress of the section at the top of the pipe.

The variation laws of stress and settlement curves before and after opening to traffic are demonstrated in Figs. 12 and 13. It is found that the curve presents a "single peak and valley" type before opening to traffic. The settlement and stress on the side of the old embankment are small, while those on the side of the new embankment are large. After opening to traffic, the curve presents a "bimodal single valley" type, the old embankment and the new embankment are symmetrical, and the corresponding settlement and stress are large, whereas the settlement and stress of the central isolation belt are small. In addition, Fig. 13 extracts the normal stress of the pipe top section of the pipeline with a forward dip angle of 0 ° from Fig, 12 for comparison with the curve after opening to traffic. The results show that the pipeline on the side of the old embankment is less affected by the opening of the new embankment (the shape of the curve is the same, and there is a slight difference in value), while the pipeline on the side of the central isolation belt and the new embankment is greatly affected by the opening of the road. Therefore, under the action of traffic load, the pipeline on the side of the central isolation zone and the new embankment will appear "leverage phenomenon"(Echoing the findings of Shi (2019) and Zhong (2019)), and the fulcrum is located at the right end of the central isolation zone (16.75 m). The normal stress of the top section of the pipeline (central isolation zone range) to the left of the fulcrum is reduced, while the normal stress of the top section of the pipeline (new embankment range) to the right of the fulcrum increases. This phenomenon exists with the stress curve and the settlement curve, and is applicable to all inclination angles of the pipeline.

7. Conclusions

Based on a road widening project in Zhejiang Province, China, this paper calculates the settlement and stress behavior of buried pipelines through finite element software and theoretical formula, and verifies the accuracy of the two methods through field measured data. Subsequently, the entire construction process, with particular focus on the settlement and stress variations of pipelines positioned at different angles to the road, is meticulously analyzed. The following conclusion can be drawn as follows:

- When widening the embankment and the traffic is open, the soil beneath the central separation zone uplifts during the slope phase, while the soil on the widened embankment side continues to settle downward.
- The settlement changes of the old and new embankments during construction were simulated by finite element software. Settlement gradually increased toward the new embankment side in the cross-sectional direction. After 15 years of construction, the total settlement of the new embankment amounted to 150 mm, significantly surpassing the 8mm settlement observed in the old embankment.
- A theoretical method has been established to calculate pipeline settlement and normal stress, considering subgrade reaction forces and consolidation of the old embankment. The overall fitting error compared to the simulation results is less than 7%.
- The settlement and stress curves of buried pipelines exhibit a "leverage phenomenon" before and after traffic flow. The fulcrum, located at the endpoint of the central isolation zone, leans toward the new embankment side. The curve transforms from a "single peak and single valley" to a “double peak and single valley” configuration.
- This study introduces a new method for calculating the settlement stress of buried pipelines and the influence of angle on pipeline settlement stress, but there are several common limitations. In the process of using software modeling, the sliding friction between the pipe and soil was not fully considered, and the theoretical methods and numerical models may need further adjustment. In addition, this study is based on ordinary pipe diameters and burial depths, and the conclusions drawn may differ from those of other minority pipe diameters and burial depths. This limitation does not diminish the value of the research, but rather provides a pathway for further investigation and improvement.

Acknowledgments

The authors would like to acknowledge the financial support from by Basic Research Project of Nantong (Grant Nos. JC22022087), the Fundamental Research Funds for the Central Universities of China (Grant Nos. B210202032) and the National Natural Science Foundation of China (Grant Nos. 52178327 and 52308348). All the above support and assistance are greatly appreciated.

References

Al-Shboul, K.F., Almasabha, G., Shehadeh, A. and Alshboul, O. (2023), “Exploring the efficacy of machine learning models for predicting soil radon exhalation rates”, *Stoch. Environ. Res. Risk A*, **37**, 4307-4321. https://doi.org/10.1007/s00477-023-02509-x.

Almadi, A. I.M., Al Mamlook, R.E., Ullah, I., Alshboul, O., Bandara, N. and Shehadeh, A. (2023), “Vehicle collisions analysis on highways based on multi-user driving simulator and multinomial logistic regression model on US highways in Michigan”, *Int. J. Crashworthines*, **28**(6), 770-785. https://doi.org/10.1080/13588265.2022.2130608.

Almasabha, G., Al-Shboul, K.F., Shehadeh, A. and Alshboul, O. (2023), “Machine learning-based models for predicting the shear strength of synthetic fiber reinforced concrete beams without stirrups”, *Structures*, **52**, 299-311.

https://doi.org/10.1016/j.istruc.2023.03.170.

Almasabha, G., Shehadeh, A., Alshboul, O. and Al Hattamleh, O. (2023), "Structural performance of buried reinforced concrete pipelines under deep embankment soil", *Constr. Innov*., https://doi.org/10.1108/CI-10-2021-0196.

Alshboul, O., Al Mamlook, R.E., Shehadeh, A. and Munir, T. (2024), "Empirical exploration of predictive maintenance in concrete manufacturing: Harnessing machine learning for enhanced equipment reliability in construction project management", *Comput. Ind. Eng*., **190**,110046. https://doi.org/10.1016/j.cie.2024.110046.

Alshboul, O., Almasabha, G., Al-Shboul, K.F. and Shehadeh, A. (2023), "A comparative study of shear strength prediction models for SFRC deep beams without stirrups using machine learning algorithms", *Structures*, **55**, 97-111. https://doi.org/10.1016/j.istruc.2023.06.026.

Alshboul, O., Almasabha, G., Mamlook, R.E.A. and Saeed Almuflih, A. (2022), "Evaluating the impact of external support on green building construction cost: A hybrid mathematical and machine learning prediction approach", *Buildings*, **12**(8), 1256; https://doi.org/10.3390/buildings12081256.

Alshboul, O., Almasabha, G., Shehadeh, A. and Al-Shboul, K. (2024), "A comparative study of LightGBM, XGBoost, and GEP models in shear strength management of SFRC-SBWS", *Structures*, **61**. https://doi.org/10.1016/j.istruc.2024.106009.

Alshboul, O., Almasabha, G., Shehadeh, A., Al Hattamleh, O. and Almuflih, A.S. (2022), "Optimization of the structural performance of buried reinforced concrete pipelines in cohesionless soils", *Material*, **15**(12), 4051. https://doi.org/10.3390/ma15124051.

Alshboul, O., Almasabha, G., Shehadeh, A., Mamlook, R.E.A., Almuflih, A.S. and Almakayeel, N. (2022), "Machine learning-based model for predicting the shear strength of slender reinforced concrete beams without stirrups", *Buildings*, **12**(8), 1166.; https://doi.org/10.3390/buildings12081166.

Alshboul, O., Alzubaidi, M.A., Mamlook, R.E.A., Almasabha, G., Almuflih, A.S. and Shehadeh, A. (2022), "Forecasting liquidated damages via machine learning-based modified regression models for highway construction projects", *Sustainability*, **14**(10), 5835. https://doi.org/10.3390/su14105835.

Alshboul, O., Shehadeh, A. and Hamedat, O. (2021), "Development of integrated asset management model for highway facilities basedon risk evaluation", *Int. J. Constr. Management*, **23**(8), 1355-1364. https://doi.org/10.1080/15623599.2021.1972204.

Alshboul, O., Shehadeh, A., Al-Kasasbeh, M., Al Mamlook, R.E., Halalsheh, N. and Alkasasbeh, M. (2021), "Deep and machine learning approaches for forecasting the residual value of heavy construction equipment: a management decision support model", *Eng. Constr. Archit. Management*, **29**(10), 4153-4176. . https://doi.org/10.1108/ECAM-08-2020-0614.

Alshboul, O., Shehadeh, A., Mamlook, R.E.A., Almasabha, G., Almuflih, A.S. and Alghamdi, S.Y. (2022), "Prediction liquidated damages via ensemble machine learning model: Towards sustainable highway construction projects", *Sustainability*, **14**(15), 159303. https://doi.org/10.3390/su14159303.

Alshboul, O., Shehadeh, A., Tatari, O., Almasabha, G. and Saleh, E. (2021), "Governmental investment impacts on the construction sector considering the liquidity trap", *J. Management Eng*., **38**(2), 1-16. https://doi.org/10.1061/(ASCE)ME.1943-5479.0001003.

Alshboul, O., Shehadeh, A., Tatari, O., Almasabha, G. and Saleh, E. (2024), "Multiobjective and multivariable optimization for earthmoving equipment", *J. Fac. Management*, **22**(1), 21-48. https://doi.org/10.1108/JFM-10-2021-0129.

Barzegar, M., Wen, H., Mivehchi, M., Akin, I.D. and Adil, T. (2023), "Investigation of excessive settlement involving recycled asphalt pavement in highway embankment", *Transp. Geotech*., **40**, 10091. https://doi.org/10.1016/j.trgeo.2023.100991.

Bin, Z., Jiang, N., Zhou, C., Luo, X., Li, H., Chang, X. and Xia, Y. (2022), "Dynamic interaction of the pipe-soil subject to underground blasting excavation vibration in an urban soil-rock stratum", *Tunn. Undeergr. Sp. Tech*., **129**, 104700. https://doi.org/10.1016/j.tust.2022.104700.

Chen G., Wang, F.T., Li, D.Q. and Liu, Y. (2020), "Dyadic wavelet analysis of bender element signals in determining shear wave velocity", *Can. Geotech. J*., **57**(12), 2027-2030. https://doi.org/10.1139/cgj-2019-0167.

Chen L., Ghorbani, J., Zhang, C. and Kodikara, J. (2022), "Stress overshooting solution for soil plasticity models", *Comput. Geotech*., **152**, 105008. https://doi.org/10.1016/j.compgeo.2022.105008.

Dong X., Zhou F., Wang X.D., *et al*. (2023), "Experimental and application of HSS model parameters in foundation pit numerical analysis", *Sci. Tech. Eng*., **23**, 7878-7885. (in Chinese)

Du, Y.J., Jiang, N.J., Liu, S.Y. and Horpibulsuk, S. (2016), "Field evaluation of soft highway subgrade soil stabilized with calcium carbide residue", *Soils Found*., **56**(2), 301-314. https://doi.org/10.1016/j.sandf.2016.02.012.

Halalsheh, N., Alshboul, O., Shehadeh, A., Al Mamlook, R.E., Al-Othman, A. and Tawalbeh, M. (2022), "Breakthrough curves prediction of selenite adsorption on chemically modified zeolite using boosted decision tree algorithms for water treatment applications", *Water*, **14**(16), 2519. https://doi.org/10.3390/w14162519.

Han, J., Oztoprak, S., Parsons, R.L. and Huang, J. (2007), "Numerical analysis of foundation columns to support widening of embankments", *Comput. Geotech*., **34**(6), 435-448. https://doi.org/10.1016/j.compgeo.2007.01.006.

Hardin, B.O. and Black, W.L. (1969), "Closure to "vibration modulus of normally consolidated clay"", *J. Soil Mech. Found. Division*, **95**(6), 1531-1537. https://doi.org/10.1061/JSFEAQ.0001364.

Jia, N., Chen, R., Chen, Y., Xu, L. and Yang, S. (2024), "Theoretical analysis and monitoring of Hangzhou Ningbo expressway expansion project", J. Geotech. Eng., **6**, 755-760. (in Chinese).

Kawa, M., Puła, W. and Truty, A. (2021), "Probabilistic analysis of the diaphragm wall using the hardening soil-small (HSS) model", *Eng. Struct*., **232**, 111869. https://doi.org/10.1016/j.engstruct.2021.111869.

Kouretzis, G. and Wu, J. (2021), "Recommendations for determining nonlinear Winkler spring parameters for buried steel pipe stress analysis applications", *Comput. Geotech*., **135**, 104196. https://doi.org/10.1016/j.compgeo.2021.104196.

Liu, L., Zhong, X. and Liao, S. (2023), "Accurate solutions of a thin rectangular plate deflection under large uniform loading", *Appl. Math. Model*., **123**, 241-258. https://doi.org/10.1016/j.apm.2023.06.037.

Liu, X., Li, Z., Zou, D., Sun, L., Yahya, K.E. and Liang, J. (2023), "Khailah Ebrahim Yahya, Jiaming Liang. Improving the prediction accuracy of small-strain shear modulus of granular soils through PSD: An investigation enabled by DEM and machine learning technique", *Comput. Geotech*., **157**, 105355. https://doi.org/10.1016/j.compgeo.2023.105355.

Luo, X., Lu, S., Shi, J., Li, X. and Zheng, J. (2015), "Numerical simulation of strength failure of buried polyethylene pipe under foundation settlement", *Eng. Fail. Anal*., **48**, 144-152. https://doi.org/10.1016/j.engfailanal.2014.11.014.

Lv, G., Cui, W., Zhang, Q., Wu, S. and Wang, S. (2021),

"Experimental study on embankment failure law and reinforcement technology for highway widening project over silt soils", *J. Test. Eval*., **49**(6), 4248-4260. https://doi.org/10.1520/JTE20200429.

Marcotte, B.A. and Fleming, I.R. (2019), "The role of undrained clay soil subgrade properties in controlling deformations in geomembranes", *Geotext. Geomembranes*, **47**(3), 327-335. https://doi.org/10.1016/j.geotexmem.2019.02.001.

Orynyak, I., Yaskovets, Z. and Mazuryk, H. (2019), "Novel numerical approach to analysis of axial stress accumulation in pipelines subjected to mine subsidence", *J. Pipeline. Syst. Eng. Pract*., **10**(4). https://doi.org/10.1061/(ASCE)PS.1949-1204.0000405.

Qin, Y., Zhu, F. and Xu, D. (2021), "Effect of the spatial variability of soil parameters on the deformation behavior of excavated slopes", *Comput. Geotech*., **136**, 104246. https://doi.org/10.1016/j.compgeo.2021.104246.

Shehadeh, A., Alshboul, O. and Almasabha, G. (2024), "Slope displacement detection in construction: An automated management algorithm for disaster prevention", *Exp. Syst. Appl*., **237**, 121505. https://doi.org/10.1016/j.eswa.2023.121505.

Shehadeh, A., Alshboul, O. and Hamedat. O. (2021), "A Gaussian mixture model evaluation of construction companies' business acceptance capabilities in performing construction and maintenance activities during COVID-19 pandemic", *Int. J. Math. Eng. Management*, **17**(2), 112-122. https://doi.org/10.1080/17509653.2021.1991851.

Shehadeh, A., Alshboul, O., Al-Shboul, K.F. and Tatari, O. (2024), "An expert system for highway construction: Multi-objective optimization using enhanced particle swarm for optimal equipment management", *Exp. Syst. Appl*., **249**, 123621. https://doi.org/10.1016/j.eswa.2024.123621.

Shi, H. (2019), Research on the Impact of Road Widening on Adjacent Buried Pipelines, Southeast University (in Chinese).

Taborda, D.M.G., Pedro, A.M.G. and Pirrone, A.I. (2022), "A state parameter-dependent constitutive model for sands based on the Mohr-Coulomb failure criterion", *Comput. Geotech*., **148**, 104811. https://doi.org/10.1016/j.compgeo.2022.104811.

Wu, Y., You, X. and Zha, S. (2019), "Mechanical behavior analysis of buried polyethylene pipe under land subsidence", *Eng. Fail. Anal*., **108**, 104351. https://doi.org/10.1016/j.engfailanal.2019.104351.

Wu, M., Cai, G., Wang, C. and Liu, S. (2022), "Mapping constrained modulus differences in a highway widening project based on CPTU data and two-dimensional anisotropic geo-statistics", *Transp. Geotech*., **32**, 100686. https://doi.org/10.1016/j.trgeo.2021.100686.

Xie, D., Guan, F. and Ding, W.Q. (2017), "Determination and sensitivity analysis of model parameters for small strain hardened soil", *J. Earthq. Eng*., **39**, 898-906.

Yang, L., Han, C., Guo, C., Cao, D., Ni, P. and Wng, F. (2022), "An innovative solution for the dynamic response of buried pipelines in layered transversely isotropic soil under pavement structures", *Comput. Geotech*., **143**, 104602. https://doi.org/10.1016/j.compgeo.2021.104602.

Yasuhiko, O., Yusuke, K. and Hiroyasu, M. (2023), "Proposition of new yield criterion for green sand mold and its experimental validation by FEM stress analysis of triaxial compression test", *J. Mater. Process. Tech*., **318**, 118020. https://doi.org/10.1016/j.jmatprotec.2023.118020.

Ye, Z., Chen, Y., Kong, G., Chen, G. and Lin, M. (2023), "3D elastodynamic solutions to layered transversely isotropic soils considering the groundwater level", *Comput. Geotech*., **158**, 105354. https://doi.org/10.1016/j.compgeo.2023.105354.

Zhang, L. and Hu, L. (2022), "Numerical simulation of electro-osmotic consolidation considering tempo-spatial variation of soil pH and soil parameters", *Comput. Geotech*., **147**, 104802. https://doi.org/10.1016/j.compgeo.2022.104802.

Zhang, Y.D. and Ron, C.W. (2023), "Effect of corrosion on buried pipe responses under external load: Experimental and numerical study", *Tunn. Undergr Sp. Tech*., **132**, 104934. https://doi.org/10.1016/j.tust.2022.104934.

Zhao, M., Liu, C., El-Korchi, T., Song, H. and Tao, M. (2019), "Performance of geogrid-reinforced and PTC pile-supported embankment in a highway widening project over soft soils", *J. Geotech. Geoenviron*., **145**(11), 06019014. https://doi.org/10.1061/(ASCE)GT.1943-5606.0002157.

Zheng, T., Zheng, L., Zhang, L., Tang, S. and Cui, Z.Y. (2021), "Safety assessment of buried natural gas pipelines with corrosion defects under the ground settlement", *Eng. Fail. Anal*., **129**, 105663. https://doi.org/10.1016/j.engfailanal.2021.105663.

Zhong, G. (2019), Research on the bearing characteristics of gas pipelines under widened roadbeds, Hunan University of Science and Technology. (in Chinese).

Zhou, H., Wang, Y.Y., Stephens, M., Bergman, J. and Nanney, S. (2018), "Tensile and compressive strain capacity in the presence of corrosion anomalies", *Proceedings of the 12th International Pipeline Conference*.

CC